Materials Physics and Mechanics 32 (2017) 152-164 Received: May 26, 2017

SHOCK-INDUCED STRUCTURAL INSTABILITIES AND SPALL-STRENGTH OF MARAGING STEELS

Yu.I. Mescheryakov*, N.I. Zhigacheva, A.K. Divakov, Yu.A. Petrov

Institute of Problems of Mechanical Engineering, Bolshoi 61, V.O., Saint Petersburg, 199178, Russia

*e-mail: ym38@mail.ru

Abstract. The shock-induced structural instability for three kinds of maraging steel is studied with two experimental techniques: Taylor technique and uniaxial strain conditions. Spall strength of steels is shown to be determined by the structural instability threshold under compression at the front of compressive pulse. Microstructure investigation of post-shocked specimens show that structural instability of maraging steel results from two factors: (i) disintegration of strengthen phase created in the process of aging of steel and (ii) shock-induced nucleation of localized austenite inclusions responsible for decrease of yield stress and fragmentation. Dynamic fracture of maraging steels is found to occur along the boundaries between shock-induced austenite laths and rest of the matrix.

Keywords: shock loading; structural instability; austenite; intermetallide; spallation.

1. Introduction

Spall fracture of material is known to be a result of interference of release waves propagating from rear surfaces of impactor and target. A common thread is that spall-strength is a characteristic of tensile strength of material at the microsecond region of dynamic loading. In reality, however, the spall strength sensitively depends on the processes flowing at the front and plateau of compressive pulse. Preliminary compression of material at the front and plateau of compressive pulse can change the structural state of material compared to its initial state. If the strain rate achieves a critical value, the irreversible structural changes of solid occur which affect the dynamic strength of material. The structural instability can be considered as a strain-rate dependent structural transition by means of which the shock self-consistently establishes the scale features of deformed medium.

The objective of paper is to establish the coupling between structural instability threshold and dynamic strength of maraging steels.

2. Experimental technique and materials

Shock tests of materials were performed with two experimental techniques. The first technique implies the plane shock loading under uniaxial strain conditions. Experimental setup for plane shock tests is shown in Fig. 1. It includes a one-stage light gas gun facility, and two-channel velocity interferometer [1]. In the majority of experiments, the thickness of target and impactor were adjusted to provide spallation. The main quantitative characteristic of material response in this technique is a time-resolved free surface velocity profile u_{fs} (t).

As example, in Fig. 2 the free surface velocity profile registered during the plane shock loading of 5 mm 38KHN3MFA steel target is presented. The velocity profile consists of several pieces, which are identified in all the experiments. Piece *OA*' is the elastic precursor, *AA*' plastic front, *AB* - transient zone, *BC* is the smooth piece of loading plastic front, *CD* is the plateau of

compressive pulse where the particle velocity is invariable, and *DF* is the unloading front. To infer the instability threshold in this technique, a series of tests at different impact velocities must be conducted. For each impact, the free surface velocity profile similar that presented in Fig. 2 is registered. Structural instability threshold is identified as impact velocity at which dependence of the free surface velocity on the impact velocity suffers a beak.

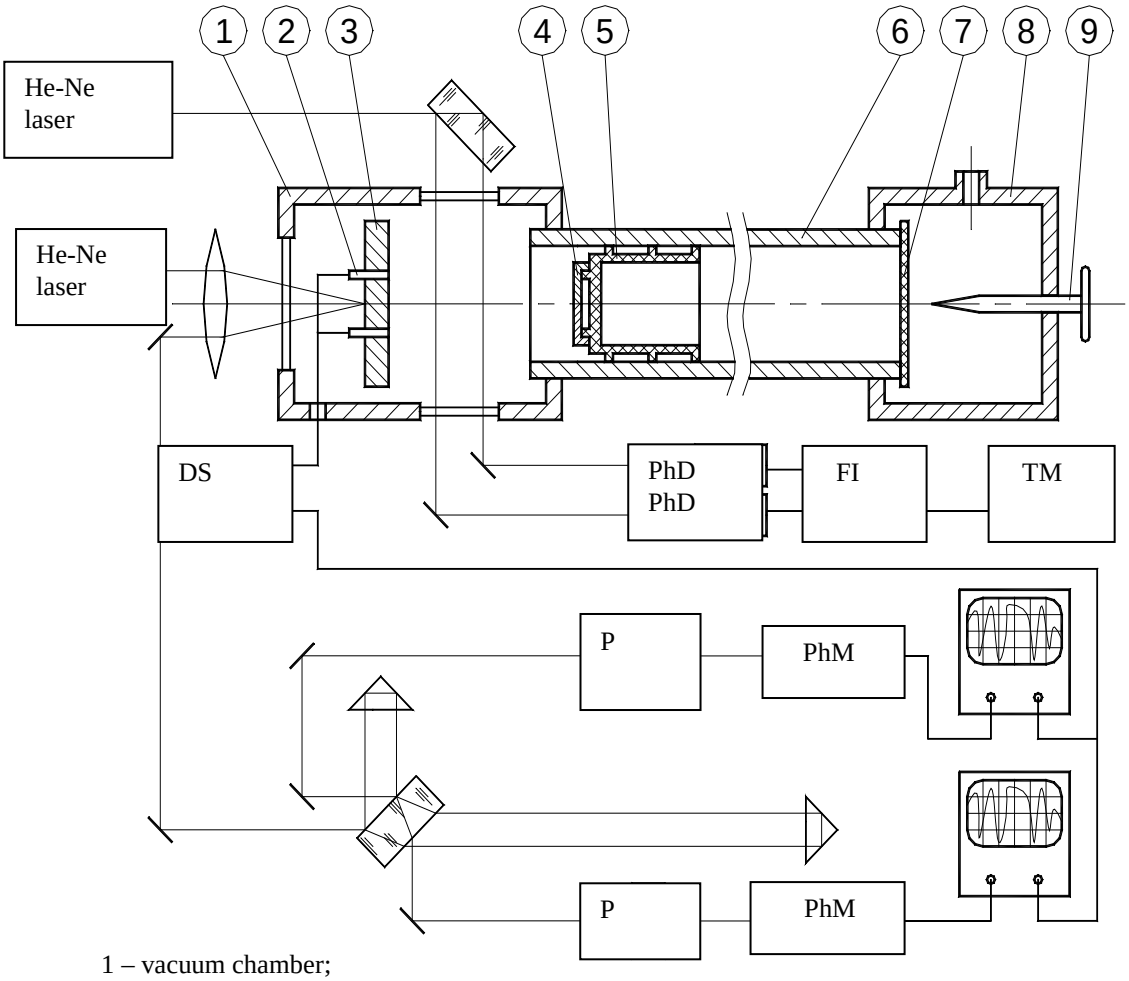

1 – vacuum chamber;
2 – pins for start of electron equipment;
3 - specimen;
4 - impactor;
5 – polycarbonate sabot;
6 - barrel;
7 - membrane;
8 - high pressure chamber
9 – facility to break the membrane.

DS – delay of start pulse;
PhD – photodetectors;
FI - device to form the pulses for time interval measurements
TM – time interval measurement device;
P - polaroids;
PhM - photomultipliers

Fig. 1. Functional scheme of experimental setup for plane shock tests.

The second experimental technique is grounded on the high-velocity collision of rod and rigid anvil. This technique has been developed by Taylor [2]. The shape of rod head reflects a response of material to dynamic load and sensitively depends on the type of dynamic stress-strain diagram [3]. In Fig. 3 two possible types of rod deformation are shown. The upper shape of rod demonstrates a gradual increase of the rod head diameter while the bottom figure shows the so-called mushroom shape of rod head.

In Fig. 4 two types of stress-strain diagram are qualitative shown. Bi-linear diagram (1) corresponds to gradual increase of rod diameter as shown in Fig.3, whereas the mushroom shape of rod head corresponds to diagram (2).

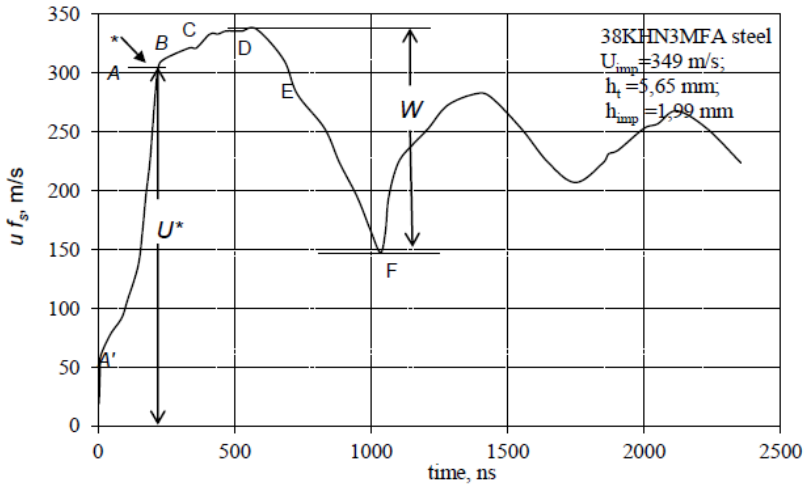

Fig. 2. Free surface velocity profile u_{fs} for 5 mm 38KHN3MFA steel target loaded at the impact velocity of 349 m/s. The break point at the plastic front is indicated by symbol*).

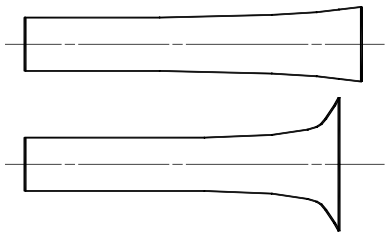

Fig. 3. Two possible types of rod deformation in Taylor tests.

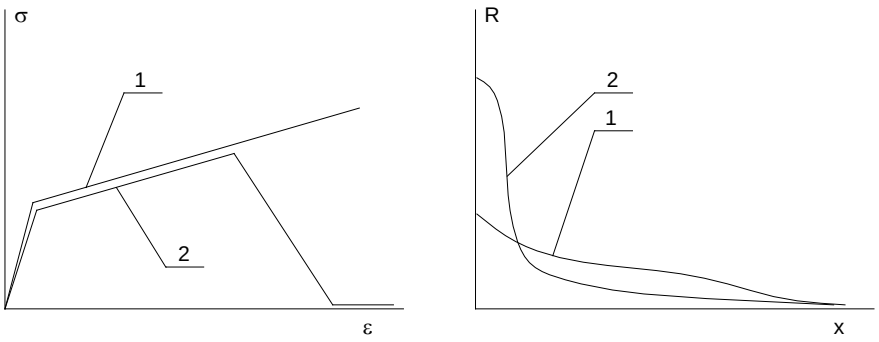

Fig. 4. Two types of stress-strain diagrams for Taylor tests.

Functional scheme of experimental setup for Taylor tests is presented in Fig. 5. The facility for Taylor tests uses the same light gas gun as that for shock tests under uniaxial strain conditions. In this setup, the hard anvil (2) manufactured from high-strength KHVG steel (hardness RCV 64) is sited inside the vacuum chamber (1). The impactor is the rod (5) which is produced from the material under investigation. The only what can be measured in this experiment is the velocity of impactor. The impact velocity when rod begins to fracture is accepted as a criterion for structural instability of material, (Table 3).

The main goal of study is to investigate the strength characteristics and structural mechanisms of fracture for maraging steels which behavior under dynamic load is unknown

and is expected to be much complex. Additional task to be solved in present study is to check whether the shock-induced structural instability threshold obtained in Taylor tests correlates with that obtained in plane shock tests. To solve this task, both Taylor tests and plane shock tests were conducted at identical strain rates with the material of well-known dynamic properties. As a test-material, 38KHN3MFA constructional steel was taken.

3. Instability threshold under compression and spall strength of materials

Determination of the strain rate at which transition to structure-unstable state of material occurs is performed by using both above experimental techniques.

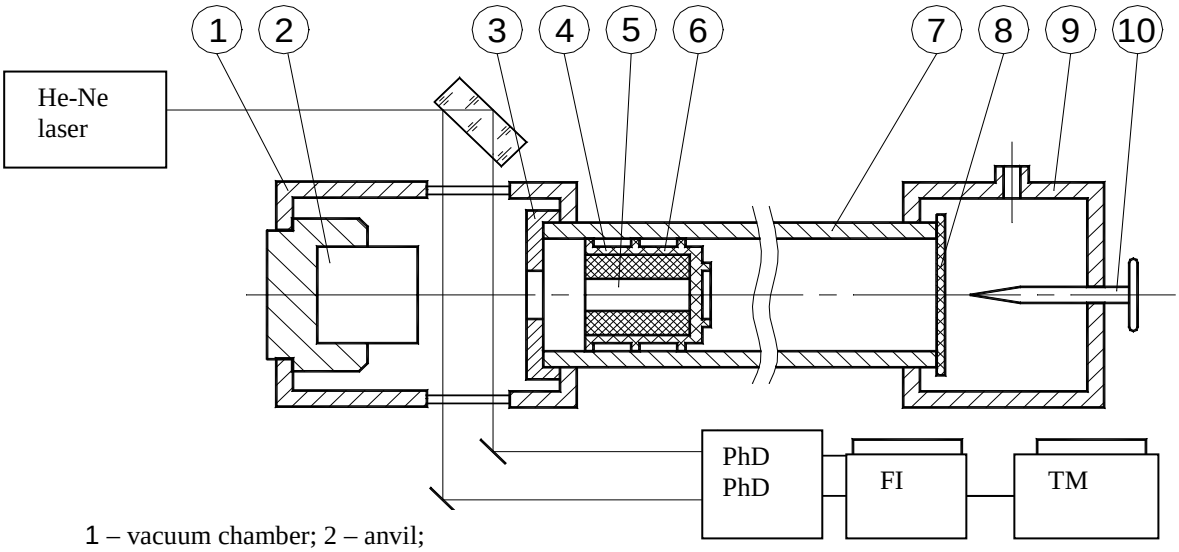

Fig. 5. Experimental setup for Taylor tests.

Chemical composition and quasistatic strength-characteristics of steels are provided in Tables 1 and 2, respectively.

Table 1. Chemical composition of materials (element: weight %).

38KHN3MFA	C: 0.36 Mn: 0.34 P: 0.022 S: 0.009 Cr: 1.29 Ni: 3.19 Mo: 042 Si: 0.29 V: 0.15 Cu: 0.08 Fe: basic
02KH18K9M5-VI	C: < 0.03 Mn: 0.5 S: 0.02 Ni: 18.5 Mo: 4.0 Si: 0.4 Co: 10.2 Ti: 0.2 Fe: basic
02KH16K9M5T1	C: < 0.015 Mn: < 0.1 P: < 0.01 S: < 0.01 Ni: 16.2 Cr: < 0.1 Co: 9 Mo: 5.2 Ti: 0.9 Fe: basic
05KH12N5K14M5TB	C: <0.02 Mn: 0.11 P: < 0.01 S: < 0.005 Ni: 5.0 Cr: 11.61 Co: 14.5 Mo: 4.67 Si: 0.005 W: 0.17 Ti: 0.44 Fe: basic

Table 2. Quasistatic strength-characteristics materials.

	$\sigma_{0.2}$, MPa	σ_b, MPa	δ, %	ψ, %	a_n
38KHN3MFA	1100	1200	12	50	80
02N18K9M5-VI	2000.3	2054	63	43.55	35-55
02KH18K9M5T1	2075-2125	2145-2185	7.4-7.6	45-47.6	45-80
05KH12N5K14M5TV	1590	1710	12.8	45.7	5-49

38KHN3MFA steel. *a). Shock tests under uniaxial strain conditions*. Results of plane shock tests under uniaxial strain conditions are provided in Table 3.

Thicknesses of target and impactor are given in the second and third columns of table, respectively. Fourth column is the impactor velocity. Maximum free surface velocity at the plateau of compressive pulse is given in the fifth column. The sixth column indicates the free surface velocity U^* at which plastic front suffers a break and transits into plateau of compressive pulse. Lastly, seventh column provides a value of pull-back velocity W which is the measure of strength of material under dynamic tensile (spall-strength). In Fig. 6 the dependencies $U^* = f(U_{imp})$ and $W = f(U_{imp})$ for 38KN3MFA steel are provided. The impact velocity at which above dependencies suffer a break we consider as the point of structural instability in shock loadings under uniaxial strain conditions.

Table 3. Results of plane shock tests for 38KHN3MFA steel.

№№ shots	h_t, mm	h_{imp}, mm	U_{imp}, m/s	U_{max}, m/s	U^*, m/s	W, m/s
1	5.68	2.06	200.9	181.3	172	-
2	5.68	2.04	239.3	221.2	207.5	169.4
3	5.68	2.10	263.1	247.8	232.7	180.7
4	5.68	2.10	306.4	282.5	247.3	160.4
5	5.68	2.09	346.7	321.2	295.0	187.1
6	5.65	1.99	349.0	337.0	311.0	189.8
7	5.62	2.02	373.5	363.9	323.3	193.3
8	5.68	2.09	404.3	390.5	335.0	203.3

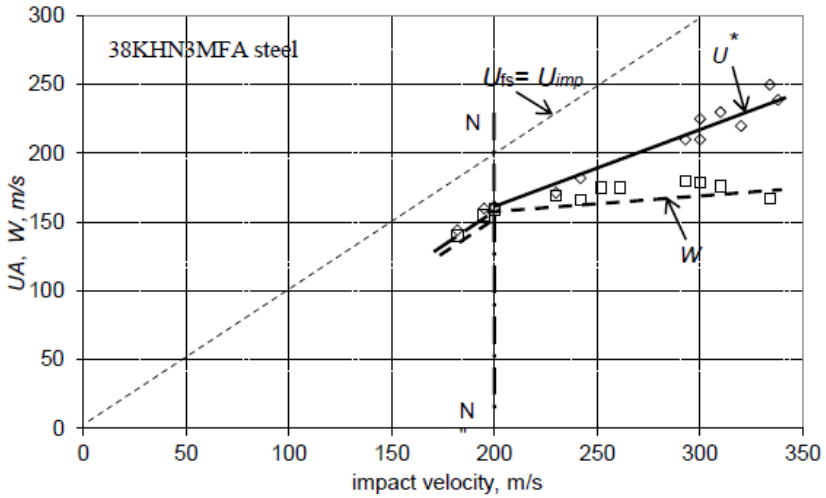

Fig. 6. Dependencies of the free surface velocity at the break point, U^*, and pull-back velocity, W, versus impact velocity for 38KHN3MFA steel.

Curve $U_{imp} = U_{fs}$, corresponds to symmetrical collision of impactor and target when acoustic impedances of impactor and target equal each other ($\rho_{imp} C_{imp} = \rho_{tg} C_{tg}$). One can see that break of dependence $U^* = f(U_{imp})$ for 38KHN3MFA steel occurs at the impact velocity of 200 m/s after what a slope of the dependence decreases. The impact velocity at which dependence $U^* = f(U_{imp})$ suffers a break, corresponds to instability threshold of material under dynamic compression, which can be considered as a shock-induced structural transition.

In Fig. 6a dependence of pull-back velocity $W = f(U_{imp})$ is also plotted. Spallation begins just at the impact velocity at which the break on the dependence $U^* = f(U_{imp})$ happens (line NN'

in Fig. 6). Irreversible structural changes in material occur at the impactor velocity of 200 m/s, which results in change of resistance to spallation.

b). *Taylor tests.* Results of Taylor tests for the 38KHN3MFA steel are provided in Table 4. Taylor tests were performed within impact velocity range from 90 m/s to 450 m/s. Within that range, there exist three stages of the rod head deformation and fracture:
1. Uniform deformation with gradual increase of the rod head;
2. Deformation and splitting of rod head by two pieces at 45°.
3. Fracture by numerous fragments.

Table 4. Result of Taylor tests for the 38KHN3MFA steel.

№№ shots	U_{imp}, mm	Y_{02}, GPa	Type of deformation (fracture)
1	89.4	1.37	uniform deformation
2	126.5	1.213	uniform deformation
3	136.6	1.65	uniform deformation
4	190.6	1.64	uniform deformation
5	206.2	1.17	uniform deformation
6	234.3	-	split under 45°
7	382.3	-	damaged
8	451.7	-	damaged

In determination, the instability threshold with Taylor tests one can use only those experimental data, which correspond to boundary impact velocity between uniform straining of rod head and beginning of fracture (shots 1-5 in Table 4). For 38KHN3MFA steel, the upper impact velocity where straining of rod head is still uniform equals 206.2 m/s. This value can be considered as critical impact velocity corresponding to structural instability threshold for the material under uniaxial stress conditions.

Thus, in Taylor tests the transition to structural instability for 38KHN3MFA steel happens approximately at the same impact velocity as in plane shock tests.

02KH18K9M5-VI maraging steel. Results of Taylor tests and plane shock tests for 02KH18K9M5-VI maraging steel are presented in Table 5 and Table 6.

a). *Taylor tests.* Depending on the character of rod deformation, the overall region of impact velocity for Taylor tests can be subdivided by three sub-regions.
1. Homogeneous dynamic straining of the rod head occurring at the impact velocities below 126.3 m/s.
2. The rod head splits by two parts in a plane inclined under 45° relatively rod axis. This occurs within velocity range from 126.3 m/s through 170 m/s.
3. Full fragmentation of the rod head which occurs from 198.4 m/s to 473.3 m/s.

Again, since the determination of yield stress and structural instability threshold in Taylor tests is correct only for the undamaged specimens, the critical impact velocity in Taylor tests for this steel is accepted to be 126.3 m/s.

b). *Uniaxial strain tests.* The instability threshold for the 02H18K9M5-ВИ maraging steel under dynamic compression and spallation is determined by using the $U^* = f(U_{imp})$ and $W = f(U_{imp})$ dependencies shown in Fig. 7. Both dependencies suffer a break at the impact velocity of 383 m/s (line NN' in Fig. 7) where the structural instability under dynamic compression is thought to occurs. As distinct from the 38KHN3MFA steel, the critical impact velocity for structural instability under uniaxial strain conditions for the 02H18K9M5-ВИ maraging steel turns out to be much higher than that for Taylor tests**.**

Table 5. Results of plane shock tests for 02KH18K9M5-VI maraging steel.

№№ shots	h_t, mm	h_{imp}, mm	U_{imp}, m/s	U_{max}, m/s	U^*, m/s	W, m/s
1	6.47	1.77	156.9	169.5	-	-
2	6.47	1.77	243.0	234.4	215.0	227.5
3	6.49	1.78	263.1	290.0	265.0	239.3
4	6.47	1.77	324.6	318.8	300.0	271.5
5	6.48	1.78	386.0	392.0	365.0	295.6
6	6.49	1.75	461.5	461.7	410.0	281.2

Table 6. Results of Taylor tests for 02KH18K9M5-VI maraging steel.

№№ shots	U_{imp}, m/s	$Y_{0.2}^{stress}$, GPa	Type of deformation (fracture)
1	51.1	3.37	uniform deformation
2	69.5	3.52	uniform deformation
3	87.4	3.42	uniform deformation
4	93.9	2.41	uniform deformation
5	126.3	3.51	uniform deformation
6	127.8	-	split under 45°
7	170.0	-	split under 45°
8	198.4	-	damaged
9	200.7	-	damaged
10	250.3	-	damaged
11	256.1	-	damaged
12	273.5	-	damaged
13	320.6	-	damaged
14	321.6	-	damaged
15	409.9	-	damaged
16	412.2	-	damaged
17	473.3	-	damaged

02N16K9M5T1 maraging steel. Results of plane shock tests and Taylor tests are presented in Table 7 and Table 8, respectively. Taylor tests can be subdivided by two sets depending on the character of deformation and fracture of the rod head.

1. Uniform straining of rod head within impact velocity range from 92.6 m/s to 153.6 m/s.
2. Fracture of rod head.

Table 7. Results of plane shock tests for 02N16K9M5T1 maraging steel.

№№ shots	h_t, mm	h_{imp}, mm	U_{imp}, m/s	U_{max}, m/s	Y, GPa	U^*, m/s	W, m/s
1	6.47	1.78	226.8	219.7	3.44	210	-
2	6.47	1.78	311.5	304.1	3.49	290	227.5
3	6.49	1.77	358.0	354.0	3.68	340	239.3
4	6.47	1.78	416.2	416.2	3.61	365	271.5

Table 8. Results of Taylor tests for 02N16K9M5T1 maraging steel.

№№ shots	U_{imp}, m/s	$Y_{0.2}^{stress}$, GPa	Type of deformation (fracture)
1	92.6	4.92	uniform deformation
2	94.2	3.75	uniform deformation
3	130.1	3.75	uniform deformation
4	153.6	2.123	uniform deformation
5	172.2	-	damaged
6	174	-	damaged
7	174.3	4.0	uniform deformation
8	175	-	damaged
9	204.8	3.72	uniform deformation
10	305.7	-	damaged
11	341	-	damaged
12	363.1	-	damaged
13	557.8	2.82	uniform deformation

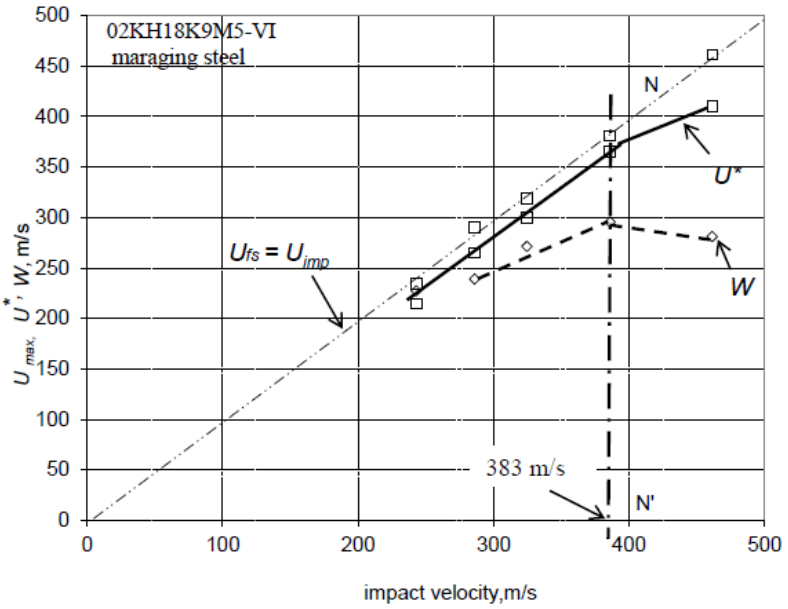

Fig. 7. Dependencies of the free surface velocity at the break-point, *U**, and pull-back velocity, *W*, versus impact velocity for 02KH18K9M5-VI steel.

The analogous value for uniaxial strain conditions resulted from the dependencies $U^* = f(U_{imp})$ and $W = f(U_{imp})$ is presented in Fig. 8.

In Taylor tests, impact velocity of 153.6 m/s can be considered as a critical velocity for initiating the structural instability of 02KH16K9M5T1 maraging steel. The critical impact velocity for structural instability in plane tests is 371 m/s, which is much higher than that for uniaxial stress conditions.

05KH12N5K14M5TV maraging steel. The third kind of maraging steel under investigation is the so-called chromium maraging steel commonly used for producing the high-pressure vessels. This steel shows the high quasistatic strength properties both at room and low temperatures. Results of plane shock tests and Taylor tests are presented in Table 9 and 10,

respectively. Structural instability threshold under uniaxial strain conditions determined from the dependencies $U^* = f(U_{imp})$ and $W = f(U_{imp})$ is indicated in Fig. 9.

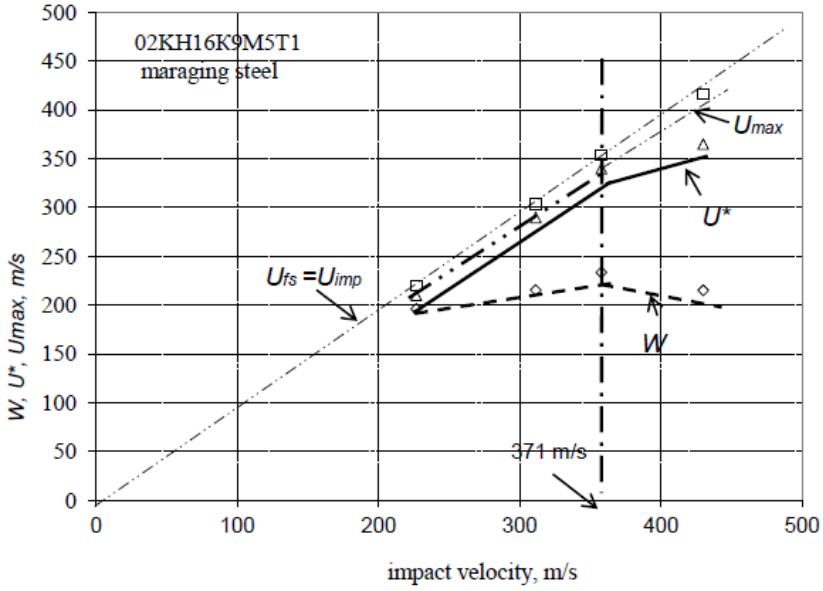

Fig. 8. Dependencies of maximum free surface velocity U_{max}, break velocity U^* and pull-back velocity W for 02KH16K9M5T1 maraging steel versus impact velocity.

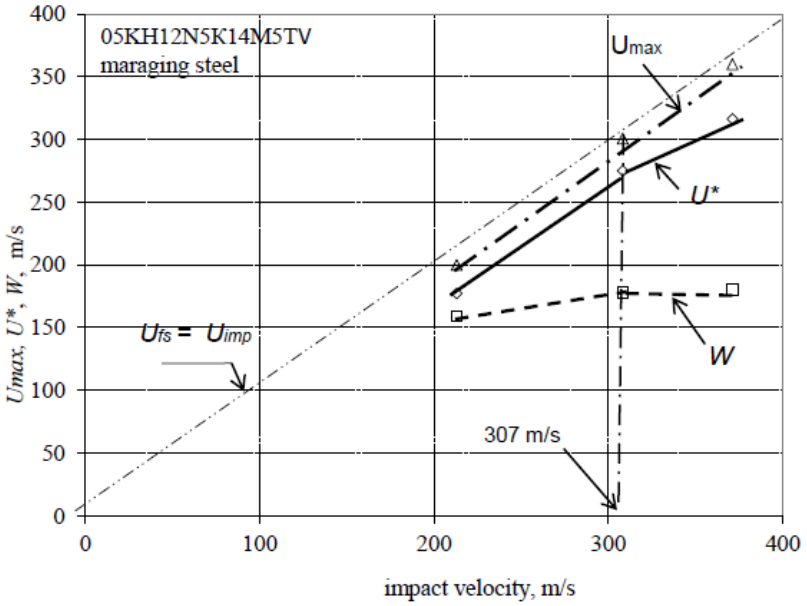

Fig. 9. Maximum free surface velocity U max, break velocity U^* and pull-back velocity W versus impact velocity for 02KH12N5K14M5TV maraging steel.

Table 9. Results of plane shock tests for 05KH12N5K14M5TV maraging steel.

№ №	*hi*, mm	h_t, mm	U_{imp}, m/s	U_{fs}^{max}, m/s	*Y*, GPa	U^*, m/s	*W*, m/s
1	5.03	1.78	213.1	201.1	2.8	177.2	159
2	5.04	1.80	308.4	300.8	2.94	275	178
3	5.05	1.79	371.3	360.0	3.29	316.4	180.4

Table 10. Results of Taylor tests for 05KH12N5K14M5TV maraging steel.

№№ shots	U_{imp}, m/s	$Y_{0.2}^{stress}$, GPa	Type of deformation (fracture)
1	93.9	1.816	uniform deformation
2	122.4	1.835	uniform deformation
3	161.9	1.925	uniform deformation
4	200.1	1.90	uniform deformation
5	237.3	2.02	uniform deformation
6	245.1	1.89	uniform deformation
7	296.3	2.11	uniform deformation
8	322.3	-	damaged
9	326	-	damaged
10	368.7	-	damaged
11	396.2	-	damaged

The critical impact velocity for structural instability of 02KH12N5K14M5TV maraging steel equals 307 m/s. It is close to that for Taylor tests (296.3 m/s). Thus, for chromium maraging steel, similar to 38KHN3MFA steel, the critical velocities for structural instability under uniaxial strain conditions and Taylor tests practically coincide

Microstructure investigations. Microstructure investigation of 02KH18K9M5-VI, 02KH16K9M5T1 and 05KH12N5H5K14M5TV maraging steels were conducted with microscope NEOPHOT-32. The measurement of microhardness were performed with PMT-3 device under load of 50 g. Etching of specimens were conducted in mixture of three acids: hydrochloric acid, nitric acid and sulphuric acid.

Structure of the first and second kinds of maraging steels is the mixture of the martensitic matrix and uniformly distributed particles of intermetallide phase. The 02N18K9M5-VI and 02KH16K9M5T1 maraging steels contain about 2 % of austenite. The third kind of steel is the stainless chromium 05KH12N5K14M5TV maraging steel which contains about 25 % austenite.

02KH18K9M5-VI maraging steel. The initial state of microstructure for this steel is presented in Fig. 10*a*. In spite of the high degree of scattering in grain size (grain size ranges from 5 μm through 50 μm), the difference in microhardness between neighbor regions of matrix equals 150 MPa whereas the mean microhardness of matrix equals 4700 MPa. Shock loading with Taylor technique leads to increase the difference in microhardness which achieves a maximum value at the impact velocity corresponding to beginning of rod head damage. So, at the impact velocity of 256 m/s the difference in microhardness equals 1650 MPa (see Fig. 10*b*).

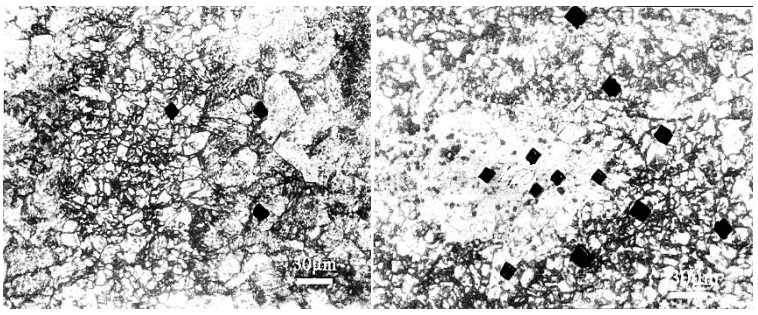

a) *b*)

Fig. 10. Structure of 02KH18K9M5-VI maraging steel in Initial state (*a*). Structure of the steel after shock loading at the impact velocity of 256 m/s (*b*). Microhardness measurements are seen in the form of black points of different size.

In Fig. 11 the microstructure of the steel after shock loading under uniaxial strain conditions at the impact velocity of 324 m/s is presented. Microhardness of matrix equals 4760 MPa whereas in damaged zone it equals 2660 MPa. Since the austenite inclusions were not found in initial state of the steel, it may be concluded that austenite inclusions are nucleated in the process of shock loading. Fracture occurs along the austenite-matrix boundaries as the most stressed regions of material (see Fig. 11). Difference in microhardness between neighbor regions of target herein is 2100 MPa.

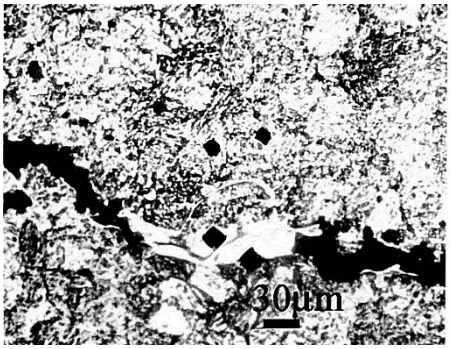

Fig. 11. Structure of the steel after shock loading at the impact velocity of 324 m/s.

02KH16K9M5T1 maraging steel. The microstructure of 02KH16K9M5T1 maraging steel is provided in Fig. 12. Mean microhardness of matrix in this steel equals 4100 MPa. Similar to previous kind of steel, the growth of difference in microhardness between neighbor regions of specimen leads to fracture of rod head. In Taylor tests, this difference ranges from 300 MPa in initial state through 1500 MPa at the impact velocity of 256 m/s.

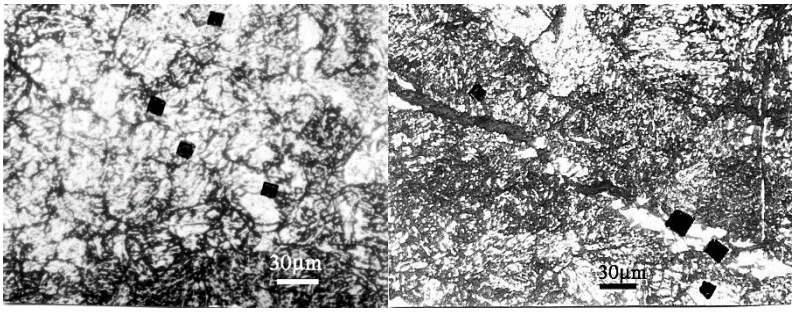

a) *b*)

Fig. 12. Initial structure of steel (*a*), structure of steel with microhardness measurements after shock loading at the impact velocity of 226 m/s (*b*).

With the increase of impact velocity up to 557 m/s, the difference in microhardness between neighbor regions begins to drop. So, the microstructure of steel at the impact velocity of 557 m/s is identical to that at the impact velocity of 130 m/s. The difference in microhardness between neighbor regions equals 450 MPa whereas dynamic deformation of rod head is uniform.

Microstructural investigations of this steel after plane shock loading at the impact velocity of 226 m/s shows that damage of specimens flows mainly along the matrix-austenite boundaries appeared in the process shocking (Fig. 12*b*). Microhardness of austenite inclusions equals 2700 MPa. Microhardness data and common character of fracture of 02KH18K9M5-VI and 02KH16K9M5T1 maraging steels evidence the presence of resonance interaction between strain rate and rate of direct and reverse alpha-gamma transformations. This interaction is thought to result in disintegration of strengthen phase created in the process of technological aging of steel.

05X12H5K14M5TB maraging steel. As distinct from the previous kinds of maraging steel, this steel has a much higher contents of Cr, which results in a large percentage of austenite in the initial state of the steel (~ 25 % instead of 2-3 % for the 02KH18K9M5-VI and 02KH16K9M5T1 maraging steels).

Microhardness of matrix equals 4530 MPa whereas the microhardness of the austenite equals 2800 MPa. Dynamic deformation of specimen in Taylor tests flows uniformly up to impact velocities of 296÷320 m/s. The head of rod in Taylor tests has a mushroom shape (see Fig. 3). The strength behavior of the steel in the velocity range is much stable although the value of yield stress is smaller than that for the previous kinds of maraging steel.

The same can be said about microstructure behavior. There is no change of microstructure state within overall range of the impact velocity of interest. Micrograph for the steel at the impact velocity of 237 m/s is identical that for the material in initial state (Fig. 13*a*). In planar tests, the behavior of this steel turns out to be much brittle (see Fig. 13*b*).

Thus, the presence of large percentage of austenite in initial state of 05KH12N5K145TV maraging steel provides the stable behavior under dynamic loading though the yield stress and critical strength threshold values decrease.

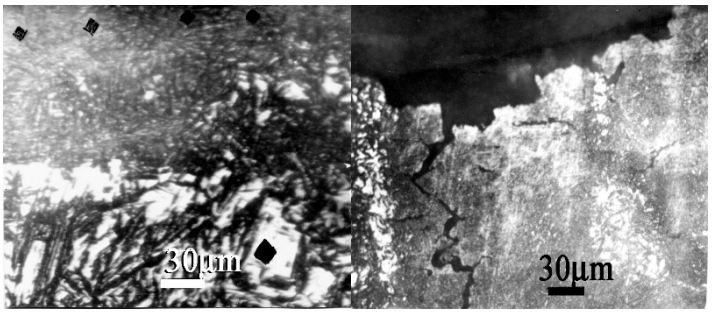

a) *b*)

Fig. 13. Initial structure of steel (*a*), structure of steel with microhardness measurements after shock loading at the impact velocity of 308 m/s (*b*).

4. Discussion

In the case of quasistatic strain rates, possibility for existence of structural transitions has been theoretically analyzed in [4]. Micro-deformation model based on solution to sine-Gordon equation predicts a non-stable behavior of crystalline lattice subjected to shear deformation in non-linear elastic region of loading. This instability leads to nucleation of large-scale structures such as meso-rotations, shear bands and their combinations. The large-scale structures appear long before the transition to macroscopic plasticity occurs. If, however, the *stress gradients* do not exceed critical value, the large-scale structures may disappear, i.e. at that stage, the structural transition turns out to be reversible. At higher strain gradients, a bifurcation transition takes place, which results in irreversible nucleation of large-scale structures.

As distinct from quasistatic condition of straining, in the case of dynamic deformation under uniaxial strain conditions, the criterion for transition of material into structure-unstable state is determined by the *strain rate*. The microstructural mechanisms responsible for structural transition were found to be the particle velocity pulsations at the mesoscale [5, 6]. In turn, amplitude of particle velocity pulsations is determined by the strain rate. Transition to structure-unstable state happens when rate of change of the particle velocity pulsations becomes higher than rate of change of mean particle velocity, which occurs just at the critical strain rate [7].

In the case of 38KHN3MFA steel and 05KH12N5K145TV maraging steel the critical impact velocities for dynamic fracture in Taylor tests and in planar tests practically coincide, which means that mechanisms for transition to structure-unstable state are identical. As for the 02KH18K9M5-VI and 02KH16K9M5T1 maraging steels, the critical impact velocity for

structural instability in Taylor tests is much lower than that for the tests under uniaxial stress conditions. In this situation, it may be supposed that an additional mechanism for transition into structure-unstable state is incorporates. For all the materials tested, the initial stage for dynamic fracture of rod head occurs along the planes of maximum tangent stress (under 45^o relatively direction of shock loading). Taylor tests turn out to be more sensitive to structural instability of material than planar tests. The reason lies in different stress state for above situations. Dynamic deformation under uniaxial strain conditions flows under high value of hydrostatic pressure whereas the shear stress constitutes only 0.05 of total normal stress [8]. The shear stress under uniaxial strain conditions is known to be equaled $\tau = \frac{1}{2}(\sigma_x - \sigma_y)$ whereas the same value under uniaxial stress conditions is $\tau = \frac{1}{2}\sigma_x$, that is much higher, since under uniaxial strain conditions σ_x and σ_y are sufficiently close. This is thought to be the reason for weak resistance of rod to splitting under dynamic compression. Another reason lies in structural specifics of 02KH18K9M5-VI and 02KH16K9M5T1 maraging steels. The above results show that 02H18K9M5-ВИ and 02H16K9M5T1 maraging steels lose their shear resistance under shock loading in Taylor tests much easily than in planar tests. Microstructure studying of specimens shows that spallation of these steels happens mainly along the boundaries of austenite inclusions nucleated during dynamic straining. As for the 38KHN3MFA steel and 05KH12N5K145TV maraging steel, their phase state after shock loading does not change. Thus, in may be concluded that structural instability of 02KH18K9M5-VI and 02KH16K9M5T1 maraging steels results from shock-induced localized phase transformation.

5. Conclusions

As a result, it can be concluded:

1. Shock tests of 02KH18K9M5-VI and 02KH16K9M5T1 maraging steels under uniaxial strain conditions and Taylor technique show that possible reason for losing the aging properties of these kinds of maraging steel at high strain rates is the shock-induced localized phase transformation
2. Where observed, the fracture mainly occurs along the shock-induced austenite laths
3. Microhardness data and common character of fracture of 02KH18K9M5-VI and 02KH16K9M5T1 maraging steels indicate a presence of resonance interaction between strain rate and rate of direct and reverse alpha-gamma transformations. This interaction is thought to result in disintegration of strengthen phase created in the process of technological aging of steels. As for the 02KH12N5K14M5TV maraging steel, the austenite phase is present in initial state of the material so the shock loading does not affect the phase state of steel.

*A**cknowledgments.** The work was performed in the frame of RNF Project 17-11-01053.*

References

[1] Yu.I. Mescheryakov, A.K. Divakov // *Dymat Journal* **1** (1994) 271.
[2] G.I. Taylor // *Proceedings of the Royal Society A* **194** (1948) 2899.
[3] V.N. Kukudjanov // *Bulletin of the Russian Academy of Sciences* **45** (1998) 388.
[4] E.L. Aero, A.N. Bulygin // *Mechanics of Solid* **5** (2007) 190.
[5] Yu.I. Meshcheryakov // *International Journal of Shock Waves* **26** (2016) 2.
[6] D.A. Indeitsev, Yu.I. Meshcheryakov, A.Yu. Kuchmin, D.S. Vavilov // *Acta Mechanica* **226** (2014) 917.
[7] Yu.I. Meshchryakov, A.K. Divakov, N.I. Zhigacheva, B.K. Barakhtin // *International Journal of Impact Engineering* **57** (2013) 99.
[8] D.E. Grady, M.E. Kipp // *Journal of the Mechanics and Physics of Solids* **35** (1987) 95.